Inorganic Chemistry

Article

pubs.acs.org/IC

Photochemistry in a 3D Metal–Organic Framework (MOF): Monitoring Intermediates and Reactivity of the *fac*-to-*mer* Photoisomerization of Re(diimine)$(CO)_3Cl$ Incorporated in a MOF

Timothy L. Easun, Junhua Jia, James A. Calladine, Danielle L. Blackmore, Christopher S. Stapleton, Khuong Q. Vuong, Neil R. Champness,* and Michael W. George*

School of Chemistry, University of Nottingham, University Park, Nottingham NG7 2RD, United Kingdom

ABSTRACT: The mechanism and intermediates in the UV-light-initiated ligand rearrangement of *fac*-Re(diimine)-$(CO)_3Cl$ to form the *mer* isomer, when incorporated into a 3D metal–organic framework (MOF), have been investigated. The structure hosting the rhenium diimine complex is a 3D network with the formula $\{Mn(DMF)_2[LRe(CO)_3Cl]\}_\infty$ (**ReMn**; DMF = *N*,*N*-dimethylformamide), where the diimine ligand L, 2,2′-bipyridine-5,5′-dicarboxylate, acts as a strut of the MOF. The incorporation of **ReMn** into a KBr disk allows spatial distribution of the *mer*-isomer photoproduct in the disk to be mapped and spectroscopically characterized by both Fourier transform infrared and Raman microscopy. Photoisomerization has been monitored by IR spectroscopy and proceeds via dissociation of a CO to form more than one dicarbonyl intermediate. The dicarbonyl species are stable in the solid state at 200 K. The photodissociated CO ligand appears to be trapped within the crystal lattice and, upon warming above 200 K, readily recombines with the dicarbonyl intermediates to form both the *fac*-Re(diimine)$(CO)_3Cl$ starting material and the *mer*-Re(diimine)$(CO)_3Cl$ photoproduct. Experiments over a range of temperatures (265–285 K) allow estimates of the activation enthalpy of recombination for each process of ca. 16 (±6) kJ mol^{-1} (*mer* formation) and 23 (±4) kJ mol^{-1} (*fac* formation) within the MOF. We have compared the photochemistry of the **ReMn** MOF with a related alkane-soluble Re(dnb)$(CO)_3Cl$ complex (dnb = 4,4′-dinonyl-2,2′-bipyridine). Time-resolved IR measurements clearly show that, in an alkane solution, the photoinduced dicarbonyl species again recombines with CO to both re-form the *fac*-isomer starting material and form the *mer*-isomer photoproduct. Density functional theory calculations of the possible dicarbonyl species aids the assignment of the experimental data in that the ν(CO) IR bands of the CO loss intermediate are, as expected, shifted to lower energy when the metal is bound to DMF rather than to an alkane and both solution data and calculations suggest that the ν(CO) band positions in the photoproduced dicarbonyl intermediates of **ReMn** are consistent with DMF binding.

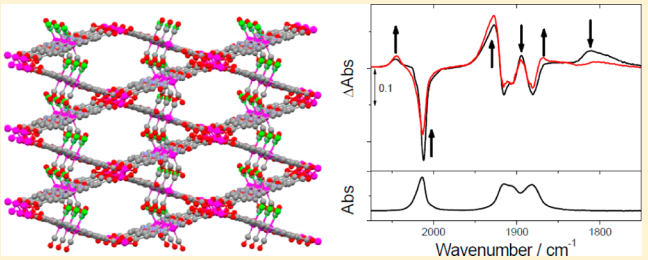

INTRODUCTION

The photochemistry of rhenium diimine complexes is of great interest for a range of applications including as photocatalysts for CO_2 reduction,[1] as photoluminescent probes for the study of DNA damage,[2] in electroluminescent devices,[3] and as luminescent components for supramolecular photochemistry.[4] *fac*-Re(bpy)$(CO)_3Cl$ (bpy = 2,2′-bipyridine) has been extensively studied, but the synthesis of the *mer* isomer was only reported in 2007, following photochemically induced CO loss in a tetrahydrofuran solution under CO. The *mer* isomer has been shown to be synthetically useful in producing novel dicarbonyls,[5] and the solution-phase photochemistry of its formation has been studied by fast spectroscopic techniques.[6]

The incorporation of photoactive metal centers into metal–organic frameworks (MOFs) is a rapidly developing area building on the applications of MOFs in magnetism,[7] gas storage,[8] drug delivery,[9] catalysis,[10] and photochemistry,[11] with studies demonstrating the ability of MOFs to stabilize unusual intermediates, taking advantage of the unusual environment and rigidity of the frameworks. Indeed, MOFs and related coordination cages provide fascinating rigid hosts that can be considered as structured matrixes for performing either chemical[12] or photochemical reactions.[13,14]

We previously reported the *fac*-to-*mer* isomerism of the Re(diimine)$(CO)_3Cl$ unit directly incorporated into the framework of a MOF.[14] This $\{Mn(DMF)_2[LRe(CO)_3Cl]\}_\infty$ (**ReMn**; L = 2,2′-bipyridine-5,5′-dicarboxylate, DMF = *N*,*N*-dimethylformamide) MOF contains the Re(2,2′-bipyridine-5,5′-dicarboxylate)$(CO)_3Cl$ unit as the linker and Mn at the nodes, forming a 3D network structure. The nature of the short-lived (picosecond to nanosecond) excited states of this *fac* isomer and the product formation (*mer* isomer) were reported, with the latter being characterized by both Fourier transform infrared (FTIR) and X-ray crystallography.

In this paper, we investigate the unsaturated *intermediates* involved in photoisomerization. A comparison with time-resolved IR studies of Re(dnb)$(CO)_3Cl$ (dnb = 4,4′-dinonyl-

Received: November 29, 2013
Published: February 11, 2014

   dx.doi.org/10.1021/ic402955e | *Inorg. Chem.* 2014, 53, 2606–2612

2,2′-bipyridine) in alkane solvents in the presence and absence of DMF is reported, and a computational study of the possible intermediates is discussed.

RESULTS AND DISCUSSION

The ground-state crystal structure of **ReMn**, which we first reported in 2010,[14] is shown in Figure 1. The extended network

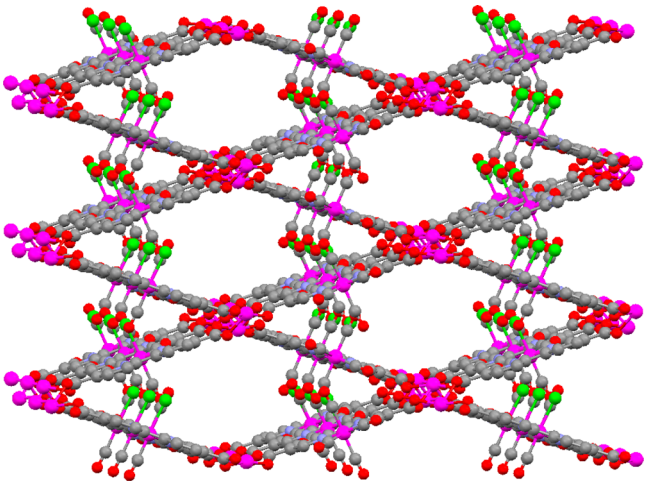

Figure 1. View of the 3D framework structure of **ReMn** showing the interlinking of $[Mn(carboxylate]_{\infty}$ chains by $[Re(diimine)(CO)_3Cl]$ moieties.

is stable in air and even at 100 °C for greater than 2 days. The MOF has been designed such that the local structural changes around the Re^{I} center are unlikely to influence the overall framework structure. The IR spectrum of **ReMn** recorded in a KBr disk displays ν(CO) bands at 2015, 1917, and 1882 cm^{-1}, consistent with the *fac* isomer of the $Re(diimine)(CO)_3Cl$ moiety. The Raman spectrum in the same conditions displays bands at 1606, 1592, 1495, 1412, 1360, and 1308 cm^{-1}.

We previously investigated[14] the effect of UV photolysis of **ReMn** in a KBr disk using FTIR imaging. Here we compare the FTIR and Raman maps of the separate disks both before and after UV photolysis at 275 K. The FTIR spectra are particularly definitive in the ν(CO) spectral region, and the Raman spectra afford further information on the backbone of the framework. The results are displayed in Figure 2. Visually, the yellow disks darken in the center, where irradiation was performed (the outer region of the disks was masked by the cell in which they were mounted). In both the FTIR and Raman spectra, notable changes are observed in this region of the disks. The IR difference spectrum obtained after 8 h of photolysis is shown in Figure 2d. The parent ν(CO) bands are clearly bleached, and several new absorptions can be seen. The FTIR experiments are consistent with our previous report of *fac*-to-*mer* isomerization within the MOF, and new ν(CO) bands are produced at 2043, 1925, and 1868 cm^{-1} because of the *mer* isomer.[13] Depletion in the *fac* ν(CO) band at 2015 cm^{-1} following 20 h of photolysis suggests that 10% of the starting *fac* isomer is photolyzed to the *mer* isomer in these experiments. Plotting the ratio of the *mer*-isomer IR band at 2043 cm^{-1} to the *fac*-isomer band at 2015 cm^{-1} affords the FTIR image of the whole KBr disk shown in Figure 2b, in which formation of the *mer* isomer in the central region of the disk can clearly be observed, in good agreement with the visual observation of the KBr disk.

We have also investigated formation of the *mer* isomer using Raman spectroscopy. The ground-state Raman spectrum (Figure 2f) shows overlapping bands in the region around 1600 cm^{-1}, which correspond to DMF bound to the Mn nodes and to the carboxylate groups of the MOF linkers. There are a series of lower-energy Raman bands (1500−1300 cm^{-1}) that correspond to ring modes of the bipyridine ligand. All of these Raman features probe the subtle changes of the framework structure upon photolysis and isomerization rather than the direct probe of metal coordination afforded by the FTIR spectra. The Raman spectral changes are shown as a difference spectrum in Figure 2f, with formation of the *mer* isomer being accompanied by a decrease in the parent band intensity around 1600 and 1500 cm^{-1} and the appearance of product bands at lower energy. Plotting the percentage of the *mer* isomer against that of the *fac* isomer affords an image showing the distribution of the *mer* isomer in the central region of the disk (Figure 2e) in much the same way as the FTIR spectral mapping experiment. This demonstrates the sensitivity of both the Raman technique and the framework to indirect structural alterations; i.e., the exchange of CO and Cl ligands around the Re center measurably affects the vibrational manifold of the MOF. This will be particularly important in future studies of MOFs that do not contain functional groups readily characterizable by IR spectroscopy.

DETERMINATION OF THE PATHWAY OF THE *FAC*-TO-*MER* ISOMERIZATION PROCESS IN REMN

The *fac*-to-*mer* isomerization in the **ReMn** MOF at 275 K proceeds via photodissociation of a carbonyl ligand to form two primary dicarbonyl intermediate(s) with ν(CO) bands at 1893, 1855, 1813, and 1794 cm^{-1}, identified by band fitting of the FTIR difference spectra using Lorentzian line shapes.[14−16] There are several possible CO-loss intermediates that can be considered as either incorporating a vacant metal site or involving coordination of an alternative ligand (see the DFT Calculations section and Figure 3). In the latter case, there are four possible octahedral geometries for $[Re(bpy)L(CO)_2Cl]$ determined by the position of both the chloride and L (axial or equatorial), which correspond to (a) ax-Cl, eq-L, (b) ax-Cl, ax-L, (c) eq-Cl, eq-L, and (d) eq-Cl, ax-L. In the case of the vacant metal site, experiments by Ishitani et al. have shown that the coordinatively unsaturated intermediate in *solution* only survives on the early picosecond time scale before reacting with solvent.[6]

The nature of our experimentally identified solid-state dicarbonyl intermediate(s) was unclear, so we investigated the effect of temperature on the reactivity and band positions of the species observed in the FTIR spectra after photolysis. In a series of experiments, the CO-loss intermediate(s) were produced by ∼20 h of photolysis of the MOF in KBr disks at 200 K. Each disk was then warmed to a specific temperature, and the thermal behavior of the photoproducts was monitored using FTIR spectroscopy. Upon warming to 275 K, the bands assigned to the CO-loss products decayed and the bands of the *fac* and *mer* isomers increased in intensity. Recovery of the *fac* isomer [k_{obs} = 8.6 (±3.0) × 10^{-5} s^{-1}] and formation of the *mer* isomer [k_{obs} = 6.1 (±1.3) × 10^{-4} s^{-1}] were each fitted to a monoexponential process. The decrease in the intensity of the dicarbonyl bands can be fitted to a biexponential decay, which correlates with the growth of *mer* and *fac* isomers, respectively [k_{obs} = 7.4 (±0.6) × 10^{-4} and 8.2 (±0.5) × 10^{-5} s^{-1}].

dx.doi.org/10.1021/ic402955e | Inorg. Chem. 2014, 53, 2606−2612

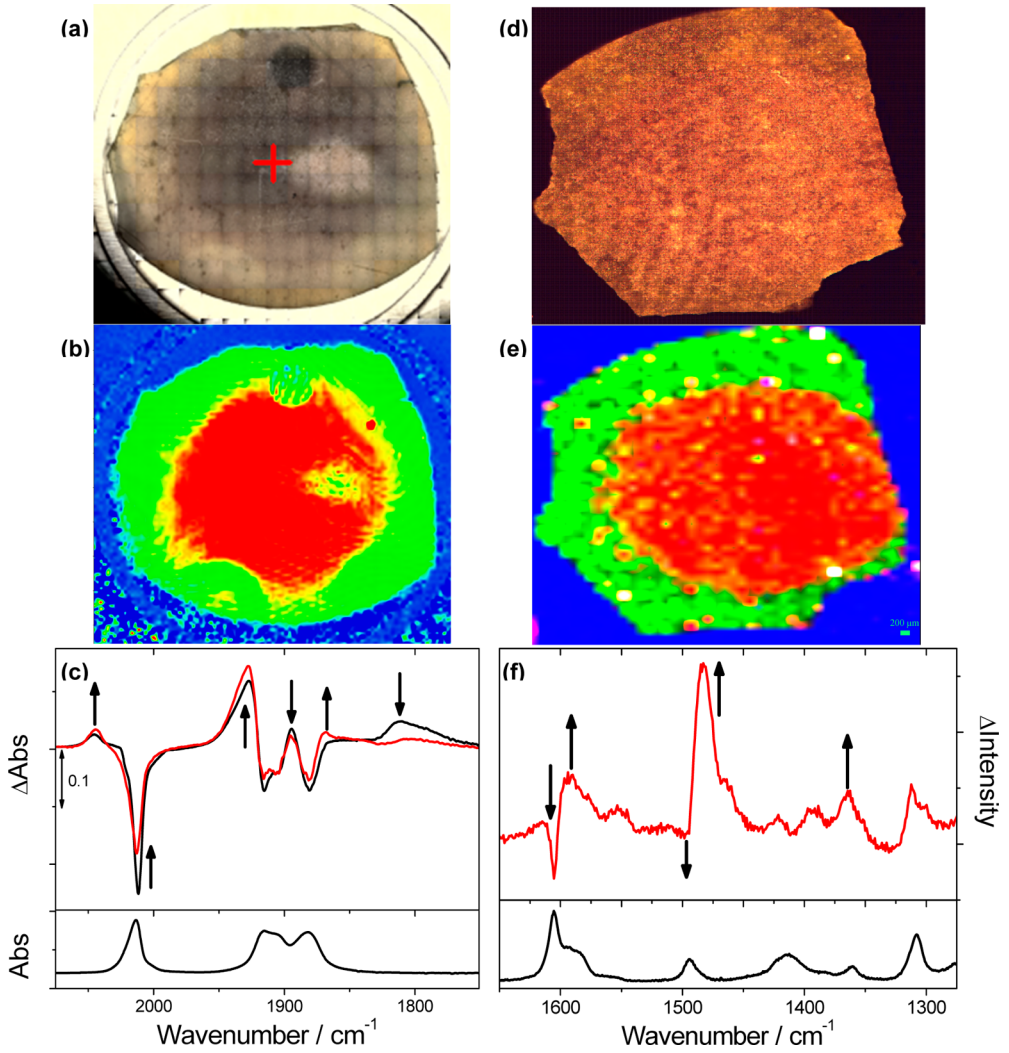

Figure 2. Results of separate FTIR and Raman mapping experiments of **ReMn** incorporated into KBr disks, following UV photolysis. (a) Optical and (b) FTIR images of the same KBr disk showing the ratio of the *mer* isomer to the *fac* isomer of **ReMn**. The red area shows the presence of the *mer* isomer, the green area shows the presence of the *fac* isomer, and the blue area is where no KBr disk is present. (c) IR difference spectrum of **ReMn** in KBr after UV photolysis at 275 K, 200 s after photolysis (black line), and 10000 s after photolysis. (d) Optical and (e) Raman images of another disk showing the regions corresponding to the presence of the *mer* (red) and *fac* (green) isomers. The blue area is where no KBr disk is present. (f) Raman difference spectrum at room temperature after UV photolysis recorded in an area where *mer*-isomer formation had occurred. (Parts a–c are reproduced with permission from ref 14. Copyright 2010 Nature Publishing Group.)

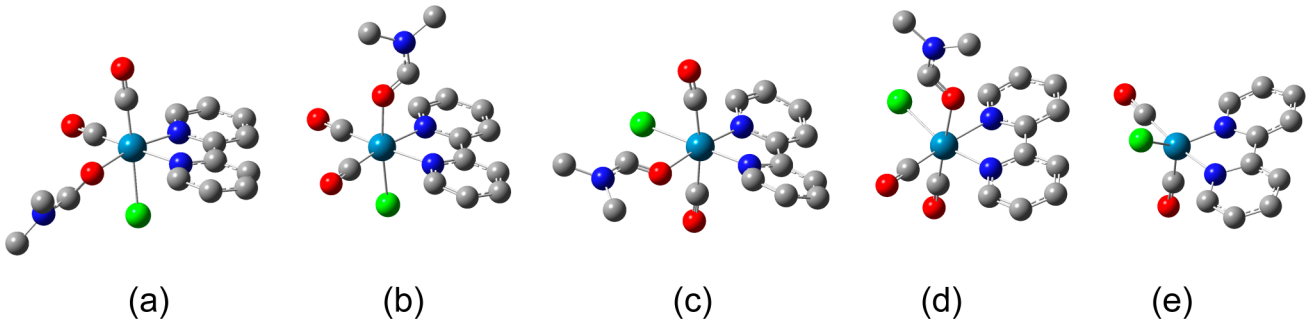

Figure 3. Possible structures (a–e; see the text) of the dicarbonyl species $[Re(bpy)(CO)_2Cl(L)]$ (where L = DMF or vacant site) calculated using DFT (H atoms have been omitted for clarity).

A more careful inspection of the spectroscopic data using band fitting reveals the presence of a ν(CO) band that decays quickly at 1813 cm^{-1} and one that decays more slowly at 1794 cm^{-1}. The different kinetic behaviors of the two CO-loss intermediates manifest themselves by the later time FTIR spectra being dominated by the lower-energy band in this region (we were not able to deconvolute satisfactorily the kinetics of the high-frequency CO-loss bands because of the heavy overlap in this region). The assignment of these two dicarbonyl intermediates can be tentatively made based on

dx.doi.org/10.1021/ic402955e | *Inorg. Chem.* 2014, 53, 2606–2612

previously reported[15] solution FTIR spectra of [Re(bpy)-$(CO)_2(CH_3CN)Cl$], with the 1893 and 1813 cm^{-1} bands being due to the $[Re(bpy)(CO)_2Cl]$ with the chloride in the equatorial position and the lower-energy 1855 and 1794 cm^{-1} pair corresponding to $[Re(bpy)(CO)_2Cl]$ with the chloride in the axial position. Further evidence for these assignments is that the former decays at the same rate as that in which the *mer* isomer grows in and the latter matches formation of the *fac* isomer, both of which are consistent with the addition of CO to the available coordination site without the need for ligand rearrangement. Once formed, the *mer* isomer is stable in the solid state at room temperature.

We have examined formation of the *mer* isomer further by determining the kinetics of dicarbonyl decay and tricarbonyl growth at specific temperatures between 260 and 285 K. Plotting these data on an Arrhenius plot (Figure 4) allows the

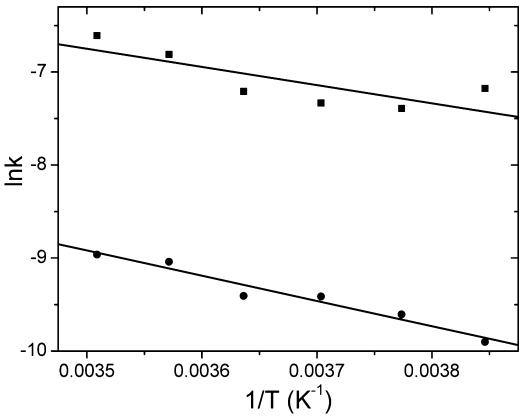

Figure 4. Plot of ln k versus $1/T$ for the fast (squares) and slow (circles) decay of the 1810 cm^{-1} band, showing linear fits to the data (solid lines).

estimation of E_a for formation of the *mer* [16 (±6) kJ mol^{-1}] and *fac* [23 (±4) kJ mol^{-1}] isomers from the dicarbonyl species. The slightly lower E_a for *mer* formation is consistent with the observed faster decay (described above) at 275 K of the bands associated with the dicarbonyl species corresponding to that with the chloride ligand in the equatorial position, i.e., predisposed toward *mer* formation (although it should be noted that these activation energies are very similar and within error).

In further experiments, we irradiated MOF-containing KBr disks at low temperature both under vacuum and under high pressure of N_2 (2000 psi) and obtained very similar results with no evidence for formation of a new dinitrogen complex. During both experiments, the formation of free CO was evident in the IR spectra at ∼2130 cm^{-1}. These results suggest that the photodissociated CO could not easily be removed from the crystalline framework and is essentially trapped within the MOF matrix.

SOLVENT-COORDINATED INTERMEDIATES IN THE ISOMERIZATION PROCESS

The crystal structure of **ReMn** shows the presence of DMF bound to the Mn nodes in the MOF. One question that arises is whether the dicarbonyl intermediates are naked or stabilized by coordination of a neighboring DMF molecule. The presence of two distinct pairs of bands for the dicarbonyl intermediates suggests that the movement of chloride is not occurring on the time scale of the experiment, possibly indicating the presence of DMF binding and the lack of a truly vacant site. The coordination of solvents to reactive intermediates produced via photochemical dissociation of CO from metal carbonyls is well established even with weakly coordinating solvents such as alkanes. With these weakly coordinating ligands, CO loss can produce long-lived organometallic alkane complexes, which can be characterized by IR and NMR spectroscopies.[17] With the strongly coordinating DMF ligand in the **ReMn** MOF, the similarity of the ν(CO) band positions of the dicarbonyls obtained after photolysis with those reported[15] for [Re(bpy)-$(CO)_2(CH_3CN)Cl$] suggests that DMF is coordinated because electron-donating solvent coordination will increase the electron density on the metal center, more than with weakly coordinating solvents such as alkanes, and shift the ν(CO)

Table 1. IR ν(CO) Band Positions of the *fac* and *mer* Isomers and Dicarbonyl Intermediates of the $[Re(diimine)(CO)_nCl]$ (n = 2, 3) Complexes in the MOF, in Solution, and as Calculated (Gas Phase)

	fac isomer ν(CO) IR bands	dicarbonyl ν(CO) IR bands	*mer* isomer ν(CO) IR bands
ReMn in a KBr disk	2015, 1917, 1882	1893, 1855, 1813, 1794	2043, 1925, 1868
$[Re(dnb)(CO)_3Cl]$ in			
DMF	2018, 1912, 1889		
cyclopentane + 10% DMF under argon	2018, 1916, 1898	1905, 1882, 1814, 1802	not obsd
cyclopentane + 10% DMF under CO	2018, 1916, 1896	1907,[a] 1883, 1814, 1804[a]	2040, 1926, 1884[b]
cyclopentane under argon and CO	2022, 1925, 1906	1922, 1915, 1902 1838, 1829, 1818	2045, 1937, 1894
Calculations[c]			
$[Re(bpy)(CO)_3Cl]$	2100, 2028, 2006		2120, 2037, 1998
$[Re(bpy)(CO)_2Cl]$ + vacant site		2070, 2028	
$[Re(bpy)(CO)_2Cl]$ + CH_4-1[d]		2019, 1967	
$[Re(bpy)(CO)_2Cl]$ + CH_4-2[d]		2022, 1960	
$[Re(bpy)(CO)_2Cl]$ + CH_4-3[d]		*e*	
$[Re(bpy)(CO)_2Cl]$ + CH_4-4[d]		2090, 2004	
$[Re(bpy)(CO)_2Cl]$ + DMF-1[d]		2004, 1955	
$[Re(bpy)(CO)_2Cl]$ + DMF-2[d]		1999, 1943	
$[Re(bpy)(CO)_2Cl]$ + DMF-3[d]		2010, 1951	
$[Re(bpy)(CO)_2Cl]$ + DMF-4[d]		2076, 1977	

[a]Uncertain band position. [b]Fitted from late-time FTIR spectrum after dicarbonyl species have decayed. [c]All frequencies are unscaled. [d]Number denotes the position of the adduct; see Figure 3, numbers 1−4 correspond to structures (a)−(d), respectively. [e]Does not optimize.

dx.doi.org/10.1021/ic402955e | Inorg. Chem. 2014, 53, 2606−2612

bands further to lower wavenumber (Table 1). Fast time-resolved IR (TRIR) spectroscopy has characterized the dissociative isomerization of [Mn(^{i}Pr-DAB)(CO)$_3$Br] (^{i}Pr-DAB = *N*,*N*′-diisopropyl-1,4-diazabutadiene), and again similar shifts in ν(CO) bands were reported upon formation of the dicarbonyl species with solvent coordinated to the vacant site.[16]

More definitive evidence could be obtained by characterizing [Re(bpy)(CO)$_2$Cl] in weakly coordinating alkane solvents to measure the smaller shifts one would predict. Unfortunately, the *fac*-[Re(bpy)(CO)$_3$Cl] precursor is insoluble in alkane solvents, and we have therefore synthesized an alkyl-substituted analogue, *fac*-[Re(dnb)(CO)$_3$Cl] (dnb = 4,4′-dinonyl-2,2′-dipyridyl), which dissolves in cyclopentane. Irradiation (266 nm) of *fac*-[Re(dnb)(CO)$_3$Cl] in cyclopentane generates a dicarbonyl species with ν(CO) bands centered around 1914 and 1828 cm^{-1}, which subsequently react with CO to form *fac*- and *mer*-[Re(dnb)(CO)$_3$Cl] (Figure 5) on a time scale of ∼1 s.

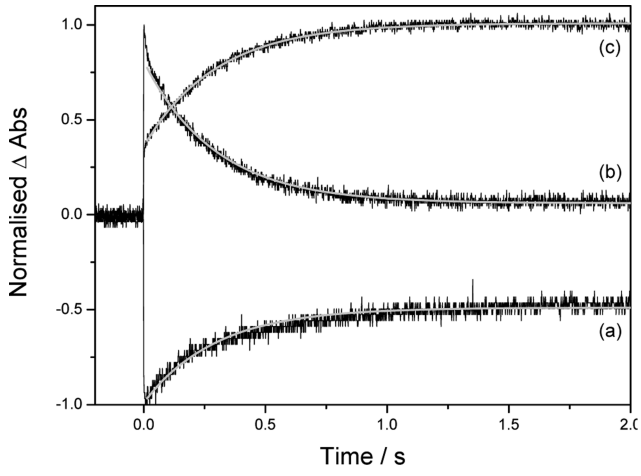

Figure 5. Kinetic traces obtained after 266 nm irradiation of *fac*-Re(dnb)(CO)$_3$Cl in cyclopentane at room temperature, in the presence of 2 atm of CO: (a) partial recovery of the parent (1926 cm^{-1}); (b) decay of the dicarbonyl (1914 cm^{-1}); (c) growth of the *mer* isomer (1938 cm^{-1}).

Doping cyclopentane with DMF (10% v/v) results in the formation of ν(CO) bands due to [Re(dnb)(CO)$_2$Cl] centered around 1900 and 1810 cm^{-1} (Table 1). These bands are ca. 16 cm^{-1} to lower energy than the dicarbonyl species observed in cyclopentane alone, while the parent absorptions shift less, by 0−10 cm^{-1} (likely indicative of a weak preferential solvation effect). Furthermore, the dicarbonyl species were long-lived in DMF (>1 h), and these results suggest that the intermediate in this case is better formulated as [Re(dnb)(CO)$_2$(DMF)Cl].

Comparing the solution results with those obtained for the **ReMn** MOF shows that the shift in ν(CO) bands in the solid-state experiment upon photolysis is consistent with DMF being bound to the metal center following photodissociation of CO. This is also consistent with the long-lived nature of these species (minutes to hours) and the slow recombination to form parent and *mer* isomers. Once the loss of dicarbonyl intermediates is complete, no further spectral changes are observed either in the solid or in the solution experiments on their respective time scales (days for the solid state and minutes for the solution phase), with the latter then being subject to diffusion of the photoproduct away from the region being monitored.

DENSITY FUNCTIONAL THEORY (DFT) MODELING OF INTERMEDIATES IN THE PHOTODISSOCIATION PROCESS

We have also performed some DFT calculations to provide more evidence for the identity of the possible intermediates involved in photodissociation. Table 1 shows the calculated ν(CO) IR band positions of *fac*-[Re(bpy)(CO)$_3$Cl], *mer*-[Re(bpy)(CO)$_3$Cl], [Re(bpy)(CO)$_2$Cl], and [Re(bpy)L-(CO)$_2$Cl] (L = CH$_4$ or a DMF molecule). As described above, there are four possible octahedral geometries for [Re(bpy)L(CO)$_2$Cl] determined by the position of both the chloride and L (axial or equatorial): (a) ax-Cl, eq-L; (b) ax-Cl, ax-L; (c) eq-Cl, eq-L; (d) eq-Cl, ax-L (Figure 3). In the DFT calculation with a vacant site only, one minimized geometry was obtained, part e, significantly distorted from octahedral. The calculated ν(CO) IR band positions are in the order [Re(bpy)(CO)$_2$Cl] > [Re(bpy)(CH$_4$)(CO)$_2$Cl] > [Re(bpy)-(DMF)(CO)$_2$Cl], consistent with the experimental observations in cyclopentane and in cyclopentane doped with 10% DMF in which the shift is ca. 16 cm^{-1} to lower energy. Furthermore, in both the [Re(bpy)(CH$_4$)(CO)$_2$Cl] and [Re(bpy)(DMF)(CO)$_2$Cl] dicarbonyl species the calculated ν(CO) bands for the isomers with axial chloride are lower in energy than those for the corresponding structures with equatorial chloride (there is one minor exception whereby the lower-energy ν(CO) band of [Re(bpy)(CO)$_2$Cl] + DMF-1 is calculated to be at 1955 cm^{-1}, but the lower-energy band of [Re(bpy)(CO)$_2$Cl] + DMF-3 is calculated to be four wavenumbers lower, at 1951 cm^{-1}). These observations further support the tentative assignment for **ReMn** above of the lower-energy pair of ν(CO) dicarbonyl bands to an intermediate in which chloride is axial, which goes on to form the *fac* isomer, and the assignment of the higher-energy pair of ν(CO) dicarbonyl bands to an intermediate in which chloride is equatorial, which goes on to form the *mer* isomer (as monitored by the kinetics).

CONCLUSIONS

The use of both FTIR and Raman mapping has demonstrated the utility of these techniques in spatially and spectrally identifying the *mer*-isomer product of the photolysis of **ReMn** in a KBr disk. We have used a combination of variable-temperature experiments, photochemistry, and FTIR spectroscopy to identify the presence of two dicarbonyl intermediates formed during photolysis. We have measured the rates of formation of the *fac* and *mer* isomers of **ReMn** from their respective dicarbonyl precursors and estimated E_a for these processes. The photolysis of [Re(dnb)(CO)$_3$Cl] in cyclopentane as a model has been used to investigate the nature of the reactive intermediates in the MOF by performing fast TRIR measurements in the presence and absence of DMF. These results were combined with DFT calculations to indicate that the dicarbonyl ν(CO) bands of the **ReMn** photoproduced intermediates are more consistent with the presence of bound DMF than the presence of a vacant site. The assignment of one intermediate to a dicarbonyl species with axial chloride (which forms the *fac* isomer upon CO addition) and the other intermediate to a dicarbonyl species with equatorial chloride (which forms the *mer* isomer upon CO addition) is consistent with the existing solution-phase literature, the matching of the dicarbonyl decay kinetics to the corresponding isomer formation on CO recombination, and the computationally

dx.doi.org/10.1021/ic402955e | *Inorg. Chem.* 2014, 53, 2606−2612

calculated differences in ν(CO) band positions for this family of reactive species.

MATERIALS AND METHODS

Rhenium pentacarbonyl chloride, 5,5′-dimethyl-2,2′-dipyridyl, and 4,4′-dinonyl-2,2′-dipyridyl were purchased from Sigma-Aldrich and used without further treatment. **ReMn** was synthesized as previously described.[14]

Preparation of [Re(dnb)(CO)$_3$Cl] and Re(C$_{31}$H$_{44}$N$_2$O$_3$Cl). The synthetic procedure used was adapted from that reported in the literature to form the unsubstituted 2,2′-bipyridine complex. [ReCl(CO)$_5$] (0.724 g, 2.00 mmol) and 4,4′-(C$_9$H$_{19}$)$_2$-2,2′-bpy (0.818 g, 2.00 mmol) were dissolved in toluene (120 mL) and heated at reflux under an atmosphere of dry argon gas for 4 h. The resulting yellow solution was cooled to room temperature and the solvent evaporated to yield a bright-yellow solid. The resulting crude product was recrystallized from hot methanol to yield a bright-yellow microcrystalline solid in two crops.

Yield: 1.17 g, 81.9%. Elem anal. Calcd for {ReC$_{31}$H$_{44}$N$_2$O$_3$Cl}: C, 52.12; H, 6.21; N, 3.92. Found: C, 52.07; H, 6.09; N, 3.99. ^{1}H NMR (CDCl$_3$, 300 MHz): δ 8.89 (d, ^3J = 5.7 Hz, 2H, H^6), 7.94 (d, ^4J = 1.3 Hz, 2H, H^3), 7.32 (dd, ^3J = 5.7 Hz, ^4J = 1.3 Hz, 2H, H^5), 2.79 (t, ^3J = 7.9 Hz, 4H, ArCH_2), 1.71 (m, 4H, ArCH$_2$CH_2), 1.43−126 (m, 24H, CH_2), 0.88 (apparent t, ^3J = 7.0 Hz, 6H, CH_3). ^{13}C NMR (CDCl$_3$, 75 MHz): δ 197.4 (aq CO), 190.1 (ax CO), 156.0, 155.7, 152.8, 127.2, 123.1, 35.9, 32.0, 30.4, 29.6, 29.5, 22.8, 14.2.

Instrumentation. The instrumentation used to record the low-temperature KBr disk spectra has previously been described elsewhere.[19] Briefly, each KBr disk was cut to fit a copper cell with CaF$_2$ windows. The cell was sealed, purged with N$_2$ gas, evacuated, attached to a coldfinger inside a vacuum shroud, and cooled to 200 K. Photolysis was achieved using a Philips HPK medium-pressure 125 W mercury arc lamp, and IR spectra were recorded on a Thermo Nicolet Avatar 360 spectrometer (with 2 cm^{-1} resolution). IR mapping was performed using a Thermo Nicolet Continuüm XL Infrared Microscope with 15× magnification. Raman mapping was performed using a Horiba Jobin Yvon LabRAM HR Raman microscope with 50× magnification and a 785 nm laser.

Point-by-point TRIR spectra were recorded on an apparatus that has been previously described elsewhere.[20] Briefly, however, a pulsed Nd:YAG laser (Spectra Physics Quanta Ray GCR 12; 266 nm) is used to initiate the reaction, and the change in the IR absorbance with time at a particular frequency is measured by an IR diode laser (Mutek MDS 1100). Kinetic measurements on a time scale longer than 1 ms (the roll off time of the detector) were achieved by direct-current coupling of the detector output to the amplifier. A solution IR cell (Harrick) with CaF$_2$ windows was fitted with customized Teflon spacers in order to limit diffusion of the photolyzed sample out of the probe beam. Samples were prepared using standard Schlenk techniques under an inert atmosphere. A fresh solution was used on each laser shot.

DFT Calculations. DFT calculations were performed using the *Gaussian 03* program at the B3LYP level of theory.[18] The effective core potential LANL2DZ was used on Re atoms, and the 6-31G(d) basis set was used on the other atoms. Frequency calculations were performed on the geometry-optimized structures.

AUTHOR INFORMATION

Corresponding Authors

*E-mail: neil.champness@nottingham.ac.uk. Tel.: +44 (0)115 9513505.

*E-mail: mike.george@nottingham.ac.uk. Tel.: +44 (0)115 9513512.

Notes

The authors declare no competing financial interest.

ACKNOWLEDGMENTS

We thank EPSRC and the University of Nottingham for financial support. M.W.G. and N.R.C. gratefully acknowledge the receipt of Royal Society Wolfson Merit Awards.

REFERENCES

(1) (a) Morimoto, T.; Nakajima, T.; Sawa, S.; Nakanishi, R.; Imori, D.; Ishitani, O. *J. Am. Chem. Soc.* **2013**, *135*, 16825−16828. (b) Doherty, M. D.; Grills, D. C.; Muckerman, J. T.; Polyansky, D. E.; Fujita, E. *Coord. Chem. Rev.* **2010**, *254*, 2472−2482. (c) Coleman, A.; Brennan, C.; Vos, J. G.; Pryce, M. T. *Coord. Chem. Rev.* **2008**, *252*, 2585−2595.

(2) (a) Smith, J. A.; George, M. W.; Kelly, J. M. *Coord. Chem. Rev.* **2011**, *255*, 2666−2675. (b) Cao, Q.; Creely, C. M.; Davies, E. S.; Dyer, J.; Easun, T. L.; Grills, D. C.; McGovern, D. A.; McMaster, J.; Pitchford, J.; Smith, J. A.; Sun, X.-Z.; Kelly, J. M.; George, M. W. *Photochem. Photobiol. Sci.* **2011**, *10*, 1355−1364. (c) Butler, J. M.; George, M. W.; Schoonover, J. R.; Dattelbaum, D. M.; Meyer, T. J. *Coord. Chem. Rev.* **2007**, *251*, 492−514. (d) Metcalfe, C.; Thomas, J. A. *Chem. Soc. Rev.* **2003**, *32*, 214−224.

(3) Si, Z.; Li, J.; Li, B.; Zhao, F.; Liu, S.; Li, W. *Inorg. Chem.* **2007**, *46*, 6155−6163.

(4) (a) Takeda, H.; Koike, K.; Morimoto, T.; Inumaru, H.; Ishitani, O. *Adv. Inorg. Chem.* **2011**, *63*, 137−186. (b) Kirgan, R. A.; Sullivan, B. P.; Rillema, D. P. *Top. Curr. Chem.* **2007**, *281*, 45−100. (c) Lees, A. J.; Sun, S. S. *Coord. Chem. Rev.* **2002**, *230*, 171−192.

(5) Sato, S.; Morimoto, T.; Ishitani, O. *Inorg. Chem.* **2007**, *46*, 9051−9053.

(6) Sato, S.; Matubara, Y.; Koike, K.; Falkenstrçm, M.; Katayama, T.; Ishibashi, Y.; Miyasaka, H.; Taniguchi, S.; Chosrowjan, H.; Mataga, N.; Fukazawa, N.; Koshihara, S.; Onda, K.; Ishitani, O. *Chem.—Eur. J.* **2012**, *18*, 15722−15734.

(7) (a) Ouellette, W.; Prosvirin, A. V.; Whitenack, K.; Dunbar, K. R.; Zubieta, J. *Angew. Chem., Int. Ed.* **2009**, *48*, 2140−2143. (b) Zhang, X.-M.; Hao, Z.-M.; Zhang, W.-X.; Chen, X.-M. *Angew. Chem., Int. Ed.* **2007**, *46*, 3456−3459. (c) Kurmoo, M. *Chem. Soc. Rev.* **2009**, *38*, 1353−1379.

(8) (a) Lin, X.; Blake, A. J.; Wilson, C.; Sun, X.; Champness, N. R.; George, M. W.; Hubberstey, P.; Mokaya, R.; Schröder, M. *J. Am. Chem. Soc.* **2006**, *128*, 10745−10753. (b) Yang, S.; Lin, X.; Blake, A. J.; Walker, G. S.; Hubberstey, P.; Champness, N. R.; Schröder, M. *Nat. Chem.* **2009**, *1*, 487−493. (c) Tan, C.; Yang, S.; Lin, X.; Blake, A. J.; Lewis, W.; Champness, N. R.; Schröder, M. *Chem. Commun.* **2011**, *47*, 4487−4489. (d) Yan, Y.; Lin, X.; Yang, S.; Blake, A. J.; Dailly, A.; Champness, N. R.; Hubberstey, P.; Schröder, M. *Chem. Commun.* **2009**, 1025−1027. (e) Farha, O. K.; Yazaydın, A. Ö.; Eryazici, I.; Malliakas, C. D.; Hauser, B. G.; Kanatzidis, M. G.; Nguyen, S. T.; Snurr, R. Q.; Hupp, J. T. *Nat. Chem.* **2010**, *2*, 944−948. (f) Lyndon, R.; Konstas, K.; Ladewig, B. P.; Southon, P. D.; Kepert, C. J.; Hill, M. R. *Angew. Chem., Int. Ed.* **2013**, *52*, 3695−3698. (g) Brown, J. W.; Henderson, B. L.; Kiesz, M. D.; Whalley, A. C.; Morris, W.; Grunder, S.; Deng, H.; Furukawa, H.; Zink, J. I.; Stoddart, J. F.; Yaghi, O. M. *Chem. Sci.* **2013**, *4*, 2858−2864.

(9) Horcajada, P.; Serre, C.; Maurin, G.; Ramsahye, N. A.; Balas, F.; Vallet-Regí, M.; Sebban, M.; Taulelle, F.; Férey, G. *J. Am. Chem. Soc.* **2008**, *130*, 6774−6780.

(10) (a) Shultz, A. M.; Farha, O. K.; Hupp, J. T.; Nguyen, S. T. *J. Am. Chem. Soc.* **2009**, *131*, 4204−4205. (b) Hwang, Y. K.; Hong, D.-Y.; Chang, J.-S.; Jhung, S. H.; Seo, Y.-K.; Kim, J.; Vimont, A.; Daturi, M.; Serre, C.; Férey, G. *Angew. Chem., Int. Ed.* **2008**, *47*, 4144−4148. (c) Fang, Q.-R.; Yuan, D.-Q.; Sculley, J.; Li, J.-R.; Han, Z.-B.; Zhou, H.-C. *Inorg. Chem.* **2010**, *49*, 11637−11642. (d) Xie, Z.; Wang, C.; deKrafft, K. E.; Lin, W. *J. Am. Chem. Soc.* **2011**, *133*, 2056−2059.

(11) (a) Lan, A.; Li, K.; Wu, H.; Olson, D. H.; Emge, T. J.; Ki, W.; Hong, M.; Li, J. *Angew. Chem., Int. Ed.* **2009**, *48*, 2334−2338. (b) Chen, B.; Wang, L.; Xiao, Y.; Fronczek, F. R.; Xue, M.; Cui, Y.; Qian, G. *Angew. Chem., Int. Ed.* **2009**, *48*, 500−503. (c) Chandler, B. D.; Yu, J. O.; Cramb, D. T.; Shimizu, G. K. H. *Chem. Mater.* **2007**, *19*,

4467−4473. (d) Modrow, A.; Zargarani, D.; Herges, R.; Stock, N. *Dalton Trans.* **2011**, *40*, 4217−4222. (e) Takashima, Y.; Furukawa, S.; Kitigawa, S. *CrystEngComm* **2011**, *13*, 3360−3363. (f) Takashima, Y.; Martinez Martinez, V.; Furukawa, S.; Kondo, M.; Shimomura, S.; Uehara, H.; Nakahama, M.; Sugimoto, K.; Kitigawa, S. *Nat. Commun.* **2011**, *2*, 168. (g) Lee, C. Y.; Farha, O. K.; Hong, B. J.; Sarjeant, A. A.; Nguyen, S. T.; Hupp, J. T. *J. Am. Chem. Soc.* **2011**, *133*, 15858−15861. (h) Fateeva, A.; Chater, P. A.; Ireland, C. P.; Tahir, A. A.; Khimyak, Y. Z.; Wiper, P. V.; Darwent, J. R.; Rosseinsky, M. J. *Angew. Chem., Int. Ed.* **2012**, *51*, 7440−7444. (i) Wang, C.; Lin, W. *J. Am. Chem. Soc.* **2011**, *133*, 4232−4235.

(12) (a) Brozek, C. K.; Dincă, M. *Chem. Sci.* **2012**, *3*, 2110−2113. (b) Haneda, T.; Kawano, M.; Kawamichi, T.; Fujita, M. *J. Am. Chem. Soc.* **2008**, *130*, 1578−1579. (c) Kawamichi, T.; Haneda, T.; Kawano, M.; Fujita, M. *Nature* **2009**, *461*, 633−635.

(13) (a) Xie, Z.; Ma, L.; deKrafft, K. E.; Jin, A.; Lin, W. *J. Am. Chem. Soc.* **2010**, *132*, 922−923. (b) Wang, C.; Wang, J.-L.; Lin, W. *J. Am. Chem. Soc.* **2012**, *134*, 19895−19908. (c) Kaye, S. S.; Long, J. R. *J. Am. Chem. Soc.* **2008**, *130*, 806−807. (d) Kawano, M.; Kobayashi, Y.; Ozeki, T.; Fujita, M. *J. Am. Chem. Soc.* **2006**, *128*, 6558−6559. (e) Easun, T. L.; Jia, J.; Reade, T. J.; Sun, X.-Z.; Davies, E. S.; Blake, A. J.; George, M. W.; Champness, N. R. *Chem. Sci.* **2014**, *5*, 539−544.

(14) Blake, A. J.; Champness, N. R.; Easun, T. L.; Allan, D. R.; Nowell, H.; George, M. W.; Jia, J.; Sun, X.-Z. *Nat. Chem.* **2010**, *2*, 688−694.

(15) (a) Kleverlaan, C. J.; Hartl, F.; Stufkens, D. J. *J. Photochem. Photobiol. A* **1997**, *103*, 231−237. (b) Kleverlaan, C. J.; Hartl, F.; Stufkens, D. J. *J. Organomet. Chem.* **1998**, *561*, 57−65. (c) Sato, S.; Sekine, A.; Ohashi, Y.; Ishitani, O.; Blanco-Rodriguez, A. M.; Vlček, A., Jr.; Unno, T.; Koike, K. *Inorg. Chem.* **2007**, *46*, 3531−3540.

(16) Vlček, A., Jr.; Farrell, I. R.; Liard, D. J.; Matousek, P.; Towrie, M.; Parker, A. W.; Grills, D. C.; George, M. W. *Dalton Trans.* **2002**, 701−712.

(17) (a) Cowan, A. J.; George, M. W. *Coord. Chem. Rev.* **2008**, *252*, 2504−2511. (b) Lawes, D. J.; Geftakis, S.; Ball, G. E. *J. Am. Chem. Soc.* **2005**, *127*, 4134−4135. (c) Calladine, J. A.; Duckett, S. B.; George, M. W.; Matthews, S. L.; Perutz, R. N.; Torres, O.; Vuong, K. Q. *J. Am. Chem. Soc.* **2011**, *133*, 2303−2310. (d) Ball, G. E.; Brookes, C. M.; Cowan, A. J.; Darwish, T. A.; George, M. W.; Kawanami, H. K.; Portius, P.; Rourke, J. P. *Proc. Natl. Sci. U.S.A.* **2007**, *104*, 6927−6932. (e) Duckett, S. B.; George, M. W.; Jina, O. S.; Matthews, S. L.; Perutz, R. N.; Sun, X.-Z.; Vuong, K. Q. *Chem. Commun.* **2009**, *11*, 1401−1403. (f) Calladine, J. A.; Torres, O.; Anstey, M.; Ball, G. E.; Bergman, R. G.; Curley, J.; Duckett, S. B.; George, M. W.; Gilson, A. I.; Lawes, D. J.; Perutz, R. N.; Sun, X.-Z.; Vollhardt, K. P. C. *Chem. Sci.* **2010**, *1*, 622−630.

(18) Frisch, M. J.; Trucks, G. W.; Schlegel, H. B.; Scuseria, G. E.; Robb, M. A.; Cheeseman, J. R.; Zakrzewski, V. G.; Montgomery, J. A., Jr.; Stratmann, R. E.; Burant, J. C.; Dapprich, S.; Millam, J. M.; Daniels, A. D.; Kudin, K. N.; Strain, M. C.; Farkas, O.; Tomasi, J.; Barone, V.; Cossi, M.; Cammi, R.; Mennucci, B.; Pomelli, C.; Adamo, C.; Clifford, S.; Ochterski, J.; Petersson, G. A.; Ayala, P. Y.; Cui, Q.; Morokuma, K.; Malick, D. K.; Rabuck, A. D.; Raghavachari, K.; Foresman, J. B.; Cioslowski, J.; Ortiz, J. V.; Stefanov, B. B.; Liu, G.; Liashenko, A.; Piskorz, P.; Komaromi, I.; Gomperts, G.; Martin, R. L.; Fox, D. J.; Keith, T.; Al-Laham, M. A.; Peng, C. Y.; Nanayakkara, A.; Gonzalez, C.; Challacombe, M.; Gill, P. M. W.; Johnson, B. G.; Chen, W.; Wong, M. W.; Andres, J. L.; Head-Gordon, M.; Replogle, E. S.; Pople, J. A. *Gaussian 03*, revision D.01; Gaussian, Inc.: Wallingford, CT, 2004.

(19) Cooper, A. I.; Poliakoff, M. *Chem. Phys. Lett.* **1993**, *212*, 611−616.

(20) Alamiry, A. H.; Boyle, N. M.; Brookes, C. C.; George, M. W.; Long, C.; Portius, P.; Pryce, M. T.; Ronayne, K. L.; Sun, X.-Z.; Towrie, M.; Vuong, K. Q. *Organometallics* **2009**, *28*, 1461−1468.